CrossMark

MOLECULAR AND CELLULAR MECHANISMS OF DISEASE

Gap-junctional channel and hemichannel activity of two recently identified connexin 26 mutants associated with deafness

Viviana Dalamon[1] · Mariana C. Fiori[2] · Vania A. Figueroa[3] · Carolina A. Oliva[3] ·
Rodrigo del Rio[4] · Wendy Gonzalez[5] · Jonathan Canan[5] · Ana B. Elgoyhen[1,6] ·
Guillermo A. Altenberg[2] · Mauricio A. Retamal[2,3]

Abstract Gap-junction channels (GJCs) are formed by head-to-head association of two hemichannels (HCs, connexin hexamers). HCs and GJCs are permeable to ions and hydrophilic molecules of up to Mr ~1 kDa. Hearing impairment of genetic origin is common, and mutations of connexin 26 (Cx26) are its major cause. We recently identified two novel Cx26 mutations in hearing-impaired subjects, L10P and G109V. L10P forms functional GJCs with slightly altered voltage dependence and HCs with decrease ATP/cationic dye selectivity. G109V does not form functional GJCs, but forms functional HCs with enhanced extracellular Ca^{2+} sensitivity and subtle alterations in voltage dependence and ATP/cationic dye selectivity. Deafness associated with G109V could result from decreased GJCs activity, whereas deafness associated to L10P may have a more complex mechanism that involves changes in HC permeability.

Keywords Deafness · Hemichannels · Connexins · Gap-junction channels · Ion channel · Mutation

✉ Mauricio A. Retamal
mretamal@udd.cl

1   Instituto de Investigaciones en Ingeniería Genética y Biología Molecular, Dr. Héctor N. Torres, Consejo Nacional de Investigaciones Científicas y Técnicas, Ciudad Autónoma de Buenos Aires, Argentina

2   Department of Cell Physiology and Molecular Biophysics, and Center for Membrane Protein Research, Texas Tech University Health Sciences Center, Lubbock, TX, USA

3   Centro de Fisiología Celular e Integrativa, Facultad de Medicina, Clínica Alemana Universidad del Desarrollo, Avenida Las Condes, 12438 Santiago, Chile

4   Centro de Investigación Biomédica, Universidad Autónoma de Chile, Santiago, Chile

5   Centro de Bioinformática y Simulación Molecular (CBSM), Universidad de Talca, Talca, Chile

6   Departamento de Farmacología, Facultad de Medicina, Universidad de Buenos Aires, Ciudad Autónoma de Buenos Aires, Argentina

Introduction

Gap-junction channels (GJCs) are aqueous channels that mediate cell-to-cell electrical and chemical coupling between adjacent cells [17, 29]. They are formed by head-to-head association of two hemichannels (HCs), one from each of the contacting cells, and are permeable to ions and hydrophilic molecules of up to Mr ~1 kDa [17, 29]. Functional HCs are connexin hexamers composed of one or more connexin isoforms. In the inner ear, the cochlea houses the organ of Corti, a narrow spiral of epithelial sensory cells (hair cells) that transduces sound waves into electrical impulses. The cochlear gap-junctional communication network includes many different cell types and is essential for hearing [2, 25, 30, 40, 47].

Hearing impairment of genetic origin is common (~1 in 2000 children), and mutations of Cx26 are its most frequent cause [23, 28, 33, 45, 46, 50]. Cx26 mutations may cause deafness by reducing gap-junctional communication [19, 21, 33, 44], which can reduce cell-to-cell permeability to signaling molecules such as inositol trisphosphate (IP₃) [6, 7, 16]. However, it has been speculated that deafness could also result from Cx26 mutations that produce "leaky" HCs [14, 23, 35, 41, 42] or decrease in HC-mediated ATP secretion into the endolymph [1, 27], although some of these mechanisms have been recently challenged [44]. In mice knockout models, the earing impairment was not associated to hair cell death [24] or loss endocochlear potential [8], but with cochlear developmental problems [8]. Moreover, specific Cx26 deletion in

🖄 Springer

Deiters cells and outer pillar cells produces hearing impairment due to a loss of high frequency response as a consequence a reduction of signal amplification [49]. Similar results were obtained in mice when Cx26 was deleted 5 days after birth, where the Cx26 knockout did not cause important changes in the cochlear morphology and endocochlear potential, but impaired active cochlear amplification, leading to late-onset hearing loss [48]. The mechanisms by which Cx26 knockout leads to these alterations remain unclear. Although not certain, it seems likely that Cx26 mutations cause deafness as a result of alterations in cell homeostasis and/or regulation that result from changes in GJC and/or HC properties. It is therefore important to identify specific alterations in deafness-associated Cx26 mutants not only because they may shed light into the mechanisms of deafness, cochlear development, and hearing, but because they may also provide information to design knockout-knocking mice models aimed at elucidating the molecular mechanisms of deafness.

We have identified two novel Cx26 missense mutations in the hearing-impaired Argentinean population, L10P (L10P, c.29T>C) and G109V (G109V, c.326G>T) [11]. In the L10P mutant, the highly conserved Leu10 in the N-terminal region is substituted with Pro. This non-conservative mutation may alter the structure of the N-terminal region, which has an important role in voltage gating [5, 26]; other mutations near L10 are also associated with deafness (the connexin deafness homepage http://davinci.crg.es/deafness/index.php). G109 is located near the interface between transmembrane helix 2 and the intracellular loop, and is not highly conserved between different isoforms, but it is among Cx26 orthologs. Although a number of mutations in transmembrane helix 2 and the intracellular loop are associated with deafness, it is presently unclear how these mutations lead to the disorder. In our previous work, L10P and G109V mutations were associated in trans with the V27I and E47X mutations, respectively [11]. V27I is a polymorphism [10, 20], whereas E47X is a nonsense mutation. These findings suggest that L10P and G109V are the underlying causes of the profound hearing impairment in the patients. However, since the complete pedigree of the patients is not available, studies to demonstrate alterations in the properties of the mutants are needed to establish their relationship to the patients' phenotype. In this work, we performed electrophysiological and permeability studies of GJCs and HCs formed by L10P and G109V and showed that the mutations produce functional alterations that could help to explain the deafness phenotype.

Materials and methods

Plasmid engineering The generation of human wild-type (WT) Cx26 DNA and cloning into the pOcyt-7 plasmid for in vitro cRNA translation has been described [9]. The human WT Cx26 DNA for mammalian expression was synthesized by Genescript and subcloned into the expression vector pF5A-CMV (Promega, Madison, WI). The L10P and G109V mutants were generated by site-directed mutagenesis (Quick Change Multisite Site-Directed Mutagenesis kit, Agilent Technologies, La Jolla, CA).

Molecular dynamics simulations The PDB of Cx26 crystal structure was used as a template [26], (PDB code: 2ZW3) for the Cx26 molecular dynamics simulations (MDS). We generated three independent MDS for WT Cx26, L10P, and G109V. For each MDS, 3 ns of thermodynamic equilibration were performed. Within this time, the HC backbone was restricted using a force of 1 kcal/mol. Then, the MDS was continued to complete 18 ns without restrictions. All MDS were performed using the NAMD program [32]. For molecular visualization, we used the program VMD [18], and to calculate the HC electrostatic charge distributions, we used the APBS module associated to VMD [3]. Changes in HC-pore radius was calculated using HOLE, an external tool called by VMD.

Cell culture HeLa cells were obtained from ATCC and were used to generate stable cell lines expressing WT Cx26, L10P, and G109V. The cells were cultured in DMEM with 10 % fetal calf serum, at 37 °C, in the presence of 5 % CO_2. Basically, cells at a confluence of 70 % were transformed with the cDNA of WT Cx26 or its mutants using lipofectamine 2000 (Life technologies) following the protocol suggested by the manufacturer. One day after transfection, the cells were exposed to 500 µg/ml of geniticine (G418, Life technologies). Non-transfected cells died after 4–5 days of exposure to G418. G418-resistant colonies were subcultured, and connexin expression was tested by Western blotting. G418 was added each time the culture media was replaced.

Dye uptake Dye uptake experiments were performed on ~80 %-confluent HeLa cells grown on a glass coverslip (#1, 12-mm radius, Marienfeld GmbH & Co, Germany). The cells were washed twice with recording solution (in mM: 148 NaCl, 5 KCl, 1.8 $CaCl_2$, 1 $MgCl_2$, 5 glucose, and 5 HEPES/NaOH, pH 7.4), and a single coverslip was placed in an inverted microscope (Nikon Ti-Eclipse) and exposed to 5 µM 2-(4-amidinophenyl)-1H-indole-6-carboxamidine (DAPI) (Life Technologies), ethidium bromide (Etd) (Sigma-Aldrich), or Yo-Pro-1 (YoPro) (Life Technologies) dissolved in recording solution. The mammalian cells divalent cation-free solution (DCFS) had the same composition as the recording solution except for the absence of $CaCl_2$ and $MgCl_2$. The rate of dye uptake was calculated from fluorescence images captured with a CCD monochrome camera (CFW-1310 M; Scion; Frederick, MD) every 30 s for

20 min, at room temperature. Once the experiment finished, we used the NIS-Elements AR Analysis imaging software (Tokyo, Japan) to create 36 ROIs overlapping cells nuclei, and linear fits of the ROIs' fluorescence vs. time were calculated using Graphpad. We have previously shown that under the conditions of our experiments, the increase in Etd fluorescence is linear with time for >20 min and can then be used as an indication of unidirectional influx [36].

cRNA preparation and injection into *Xenopus laevis* oocytes Isolation of *Xenopus laevis* oocytes, synthesis of cRNA, and oocyte injection were performed as described [34]. Oocytes were injected with 12.5 ng of antisense Cx38 oligonucleotide alone to reduce endogenous expression of Cx38 (control) or combined with WT Cx26 and/or L10P or G109V cRNAs (generally 25 ng). After cRNA injection, the oocytes were maintained in Barth's solution (in mM, 88 NaCl, 1.0 KCl, 0.4 $CaCl_2$, 0.3 $Ca(NO_3)_2$, 0.8 $MgCl_2$, and 10 HEPES/NaOH, pH 7.40) supplemented with 0.1 mg/ml gentamicin, 20 units/ml penicillin, and 20 μg/ml streptomycin. Experiments were carried out 2–3 days after injection. Plasma-membrane expression of WT Cx26, L10P, and G109V was assessed by immunoblotting of biotinylated oocyte plasma membranes; twenty oocytes/conditions per experiment were incubated with a cell-impermeable biotinylation reagent (EZ-Link Sulfo-NHS Biotin, Pierce Biotechnology, Rockford, IL) for 30 min at room temperature, and biotinylated membrane proteins were isolated based on the biotin-streptavidin interaction, essentially as described [4, 9] Enriched plasma membranes obtained from four oocytes per condition were probed with a mouse anti-Cx26 antibody directed against the intracellular loop (Life Technologies, Carlsbad, CA). The secondary antibody was a horseradish peroxidase-labeled goat anti-mouse antibody (Life Technologies), and detection was by chemiluminescence. All the experiments in *Xenopus Laevis* were conducted following the guidelines of the Clinica Alemana Universidad del Desarrollo committee for care and use of animal. The protocol was approved by this committee for the Fondecyt grant (N°1120214). All surgeries were performed under 1 % tricainemethasulphonate anesthesia, and all efforts were made to minimize suffering.

Electrophysiological recordings HC currents were measured in oocytes bathed at room temperature with ND96 solution, as described [34]. The ND96 solution contained 96 mM NaCl, 2 mM KCl, 1.8 mM $CaCl_2$, and 5 mM HEPES/NaOH, pH 7.4. Activation of HCs was accomplished by bathing the cells in nominally Ca^{2+}-free ND96 solution (DCFS; in mM, 88 NaCl, 1.0 KCl, and 10 HEPES/NaOH, pH 7.40). Data acquisition and analysis were performed with pClamp 10/Digidata 1440A A/D Board (Molecular Devices,

Foster City, CA). Currents were elicited by 15-s square pulses, ranging from −60 to +60 mV, in 10-mV steps, from a holding voltage of −60 mV, with 10-s intervals between pulses. For GJC current (Ij) measurements in paired oocytes, the vitelline membrane was manually removed 1 day after cRNA injection. The oocytes were then paired with the vegetal poles facing each other and incubated in Barth's solution for at least 24 h prior to the electrophysiological measurements using the dual two-microelectrode voltage clamp technique, as described [34]. The paired cells were clamped at −40 mV, and a transjunctional potential (V_j) was generated by stepping the voltage of one cell from −40 mV, while holding constant the voltage of the other cell (used as reference). The current supplied to the cell clamped at −40 mV is equal in amplitude, but opposite in sign, to Ij. Currents were recorded upon stepping the Vj from −100 to 100 mV for 15 s, at 20-mV intervals, and with 15-s intervals between pulses.

ATP measurements ATP released from HeLa cells was determined using a bioluminescence assay kit (Sigma-Aldrich, St. Lois, MO), and the light emission was measured in a spectrofluorometer (Jasco Corp., FP-63000, Tokyo, Japan) without excitation light. Cells were seeded into 60-mm culture dishes until they reached 70 % confluence. Then, the culture medium was removed, and the cells were washed twice with DCFS or recording solution (control conditions). The cells were then incubated in DCFS to induce ATP release. After 5 min, 500 μl of extracellular solution was carefully collected and placed on ice. To measure the ATP content of each sample, 50 μl of the extracellular solution was mixed with 50 μl of luciferin/luciferase reagent, and the light signal was measured for 10 s at 560 nm. ATP concentration was calculated from a luminescence standard curve, and data were normalized by the total cell protein of each plate.

Western blots HeLa cells and oocytes were placed in ice-cold phosphate-buffered saline solution (PBS) containing a protease and phosphatase inhibitors cocktail (#88668, Pierce, Rockford, IL). Then, cells were lysed by sonication, and protein content was determined with the Coomassie protein assay (Thermo Scientific, Rockford, IL, USA). The cell lysate was resuspended in Laemmli buffer and resolved in a NuPage 10 % SDS Bis-Tris gel (Life Technologies, Carlsbad, CA). After electrophoresis, proteins were transferred to a PVDF membrane and incubated in PBS-BLOTTO (5 % nonfat milk) for 45 min. Then, the PVDF membranes were incubated with the anti-Cx26 polyclonal antibody (Life Technologies) overnight at 4 °C, followed by several washes in TBS plus 1 % tween 20, and then incubated with horseradish peroxidase-conjugated goat anti-rabbit IgG (secondary

antibody) for 1 h at room temperature. An ECL SuperSignal kit was used according to the manufacturer's instructions (Life Technologies) to detect immunoreactivity by chemiluminescence using a C-DiGit Chemiluminescent Western Blot Scanner (Li-COR, Lincoln, NE). Each Western blot membrane was stripped with Restore Western blot stripping buffer (Thermo Scientific) for 60 min, washed with TBS plus 1 % tween 20, and incubated in PBS-BLOTTO (5 % nonfat milk) for 45 min before re-probing to detect the levels of the housekeeping protein tubulin (monoclonal anti-β tubulin antibody, Pierce). Tubulin was used to normalize the expression of WT Cx26, L10P, and G109V.

Statistical analysis Results are expressed as means ± SEM, and n refers to the number of experiments. Significance was determined using a one-way ANOVA or paired Student's t test, as appropriate. Differences were considered significant at $P < 0.05$.

Results

Cx26 L10P and G109V mutants form functional hemichannels

The approximate location of the mutations is presented in a schematic representation and the structure of Cx26 (Fig. 1a, b). Both L10 and G109 are highly conserved in Cx26 orthologs (Fig. 1c). The expression of WT and the L10P and G109V mutants in *Xenopus* oocytes did not reveal obvious differences in expression or electrophoretic motility (Fig. 2). A similar analysis in HeLa cells showed that the expression of the L10P and G109V mutants was higher than that of WT Cx26 (3.3 ± 0.3 and 2.0 ± 0.3-fold higher than WT, respectively, $n = 3$). These results indicate that the WT Cx26 and mutants are expressed in both systems, allowing us to proceed with the functional studies.

In HeLa cells studied in divalent cation-free solution (DCFS, see Materials and methods for composition), the
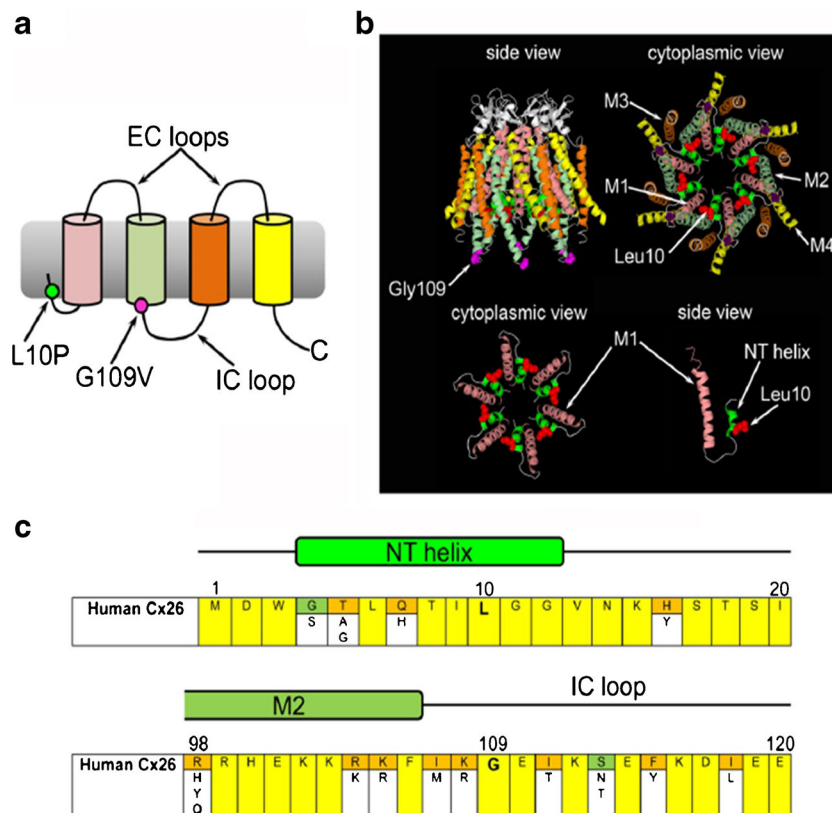

Fig. 1 Cx26 structure and sequence. **a** Schematic representation of Cx26. The intracellular loop (IC loop), extracellular loops (EC loops), and C-terminal region (C) are labeled. *Filled circles* denote the approximate location of the L10P (*green*) and G109V (*red*). **b** Structure of the Cx26 hemichannel. The bottom images show only M1 and the N-terminal region of a monomer. Color code: N-terminal helix in *green*, L10 in *red* (space-filling representation), M1 in *pale pink*, M2 in *pale green*, G109 in *cyan* (space-filling representation), M3 in *orange*, and M4 in *yellow*. **c** Homology between primary sequences of mammalian Cx26 orthologs. The regions around L10P and G109V are shown. The graph displays the summary of the alignment analysis of twenty-two mammalian Cx26 orthologs against human Cx26. The highlighted residues depict identities of 100 % (*yellow*), 79–96 % (*orange*), and 54–65 % (*green*). The *letters in the white boxes* indicate residues that can be found at the corresponding positions in the orthologs. The *numbers at the top* denote positions in the human Cx26 sequence. The Cx26 sequences analyzed were from alpaca, armadillo, microbat, cat, cow, chimpanzee, dog, dolphin, elephant, galago, gorilla, guinea pig, hyrax, kangaroo rat, macaque, mouse, mouse lemur, orangutan, pika, rabbit, rat, and shrew
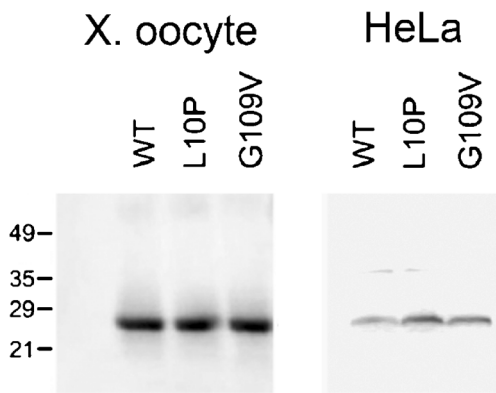
Fig. 2 Plasma membrane expression of WT Cx26 and the Cx26 mutants L10P and G109V. Representative immunoblots of lysates (50-μg protein) from Xenopus oocytes ($n = 4$) and HeLa cells ($n = 3$) probed with a specific anti-Cx26 antibody. Molecular weights of WT Cx26 and mutants were similar, and all of them migrated at ~26 kDa. Left panel: oocytes were injected with anti-Cx38 antisense oligonucleotide together with cRNA coding for Cx26 (*WT*) or the Cx26 mutants L10P (*L10P*) or G109V (*G109V*). Right panel: HeLa cells stably transfected with WT Cx26 or the mutants L10P or G109V. *Labels on the right* correspond to molecular weight markers (in kDa)

HCs formed by WT Cx26 or its mutants were permeable to Etd (MW 314; net charge +1), DAPI (MW 350; net charge + 2), and YoPro (MW 629; net charge +2) (Fig. 3). The rates of uptake of the three dyes in the cells expressing L10P were 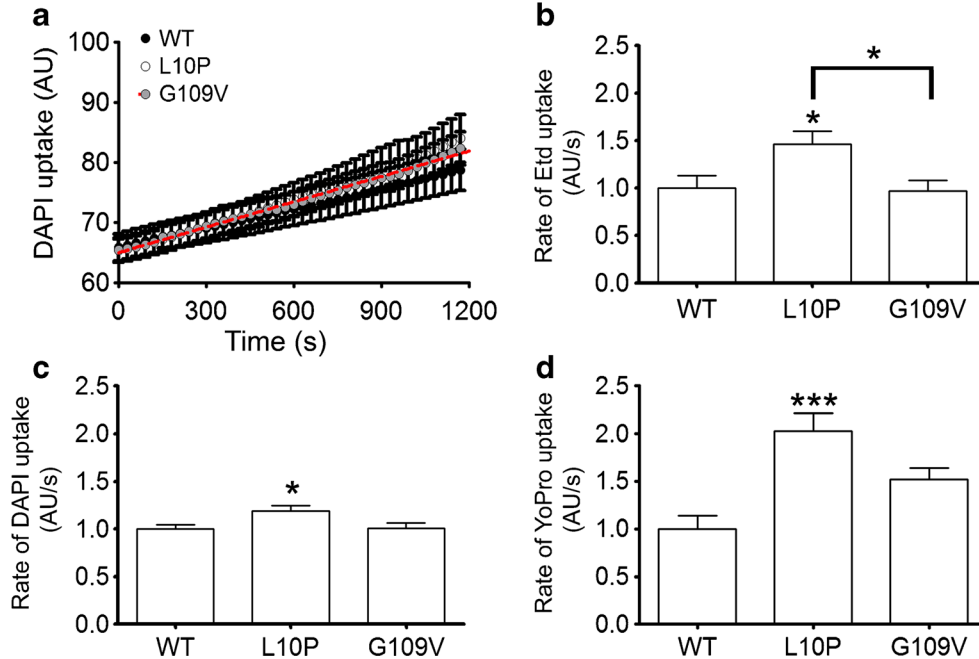significantly higher than those in cells expressing WT Cx26, but the uptakes in the cells expressing G109V were not (Fig. 3). The effects of maneuvers known to inhibit HCs [37] were assessed to determine whether the regulation and/ or inhibition of the HCs was altered by the mutations. Both mutants showed increased inhibition by Ca^{2+}. Compared to DCFS, 1.2-mM extracellular Ca^{2+} decreased the rate of DAPI uptake by ~35, ~57, and ~71 % for WT Cx26, L10P, and G109V HCs, respectively (Fig. 4a). HCs are known to be blocked by extracellular divalent cations [15, 43]. In contrast, exposure to acidic DCFS (pH reduced from 7.4 to 6.5), a condition that reduces HC opening [38], produced the same degree of inhibition in the WT Cx26 and mutant HCs (Fig. 4b). Finally, the HC inhibitor gentamicin (200 μM) [12] produced a similar decrease in the rate of DAPI uptake through WT Cx26 and G109V HCs (>50 %), but only about ~10 % inhibition of L10P HCs (Fig. 4c). These observations show that the L10P and G109V mutations produce HCs with increased sensitivity to Ca^{2+}, and suggest that the N-terminal region is involved in the HC inhibition by aminoglycosides.

Since Cx26 HCs are permeable to ATP [13] and efflux of the nucleotide through HCs seems to be important for hearing processing [1], we also determined the permeation of the nucleotide through the mutant HCs. We found that switching from medium containing 1.2 mM Ca^{2+} to DCFS increased ATP release from HeLa cells expressing WT Cx26 or the L10P or G109V mutants (Fig. 5a). There were no significant

Fig. 3 Dye uptake in cells expressing WT Cx26, L10P, and G109V. **a** Representative recordings of DAPI uptake (5 μM in DCFS) in HeLa cells expressing WT Cx26 or the mutants L10P or G109V. The DAPI uptake was linear for at least 20 min. Pictures were taken every 20 s, and the rate of DAPI uptake was calculated by linear fitting of the fluorescence data. The *dashed red line* corresponds to the fit of the G109V data, as an example. **b** HeLa cells in DCFS were exposed to Etd, DAPI, or YoPro at a final concentration of 5 μM. The *bars* represent the means ± SEM of four independent experiments for Etd, ten independent experiments for DAPI, and five independent experiments for YoPro. The data were normalized to the average value in cells expressing WT Cx26. A minimum of 36 cells was analyzed for each experiment. * and *** denote $P < 0.05$ and $P < 0.001$, respectively

differences in the release of ATP between the cells expressing WT Cx26, L10P, or G109V. When ATP release or dye uptake was normalized to the relative amount of connexin (see Fig. 2), all fluxes in cells expressing L10P and G109V HCs were are at least 50 % lower than those in cells expressing WT Cx26 HCs (not shown). The decrease in ATP release in 1.2-mM Ca^{2+} medium in the cells expressing G109V is consistent with the increased response of this mutant to the inhibitory effect of Ca^{2+} on DAPI uptake (Fig. 4); the value in L10P-expressing cells was also lower, but the difference was not statistically significant. Transport data between cells expressing Cx26 and mutants are always difficult to compare not only because of differences in expression levels at the plasma membrane vs. total expression, but also because of uncertainty about the fraction of plasma-membrane connexins that forms active HCs. To determine alterations in HC permeability properties that are independent of the number of active HCs, we calculated the ATP/dye flux ratios. The data in Fig. 5b show that compared to WT Cx26, the L10P HCs display lower ATP/dye selectivity. Another noticeable difference was that the ATP/YoPro selectivity of G109V HCs was lower than the ATP/Etd and ATP/DAPI selectivities, indicating that G109V HCs have a higher relative permeability to YoPro vs. Etd and DAPI. Overall, the results suggest that L10P and G109V do form functional HCs, and that L10P HCs display clear alterations in relative permeabilities to the negatively charged ATP vs. cationic dyes, whereas the changes in G109V HCs selectivity are more subtle.

To confirm that L10P and G109V form functional HCs, we measured voltage-gated HC currents [39]. Under control conditions (1.2-mM extracellular $[Ca^{2+}]$), the currents measured in *Xenopus* oocytes injected only with antisense against the endogenous Cx38 were not different from zero (0.02 ± 0.04 μA), but increased to 1.29 ± 0.15 μA in DCFS (Fig. 6a; $n = 8$). In oocytes expressing WT Cx26, the HC currents under the control conditions and in DCFS were clearly observed, with values of 2.32 ± 0.11 and 6.49 ± 0.67 μA, respectively (Fig. 6b). In DCFS, WT Cx26 showed a current

Fig. 5 Efflux of ATP through WT Cx26, L10P, and G109V HCs. **a** HeLa cells were exposed to the DCFS or control solution containing 1.2 mM Ca^{2+}, and ATP released from the cells into the extracellular solution was measured using a luciferin/luciferase-based assay. Data are presented as means ± SEM ($n = 3$ for each set) normalized to the average value in cells expressing WT Cx26 under the corresponding condition. There were no statistically significant differences between the release of ATP through WT Cx26 and mutant HCs in DCFS, but the values in DCFS were significantly higher than those in 1.2 mM Ca^{2+} ($P < 0.05$). **b** Ratio of the ATP release/dye uptake measured in DCFS. Each ratio was normalized to the WT Cx26 average to facilitate comparisons. See Figs. 3b–d and 5a for details. * and *** denote $P < 0.05$ and $P < 0.001$, respectively

inactivation time constant of 3639 ± 420 ms at +50 mV. L10P HC currents under the control conditions were very similar in shape and amplitude (2.20 ± 0.23 μA) to the WT Cx26 HC currents. However, L10P HC currents in DCFS
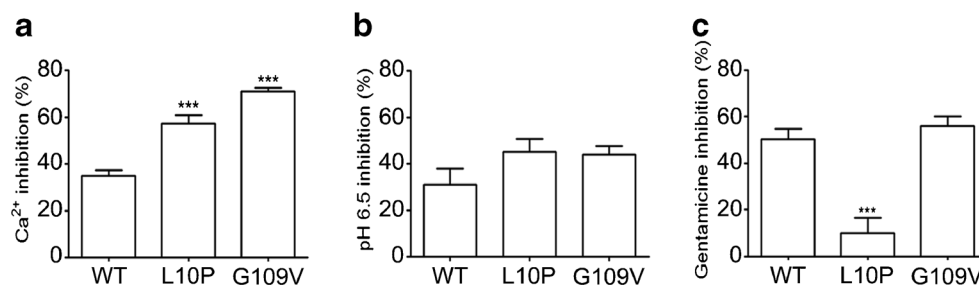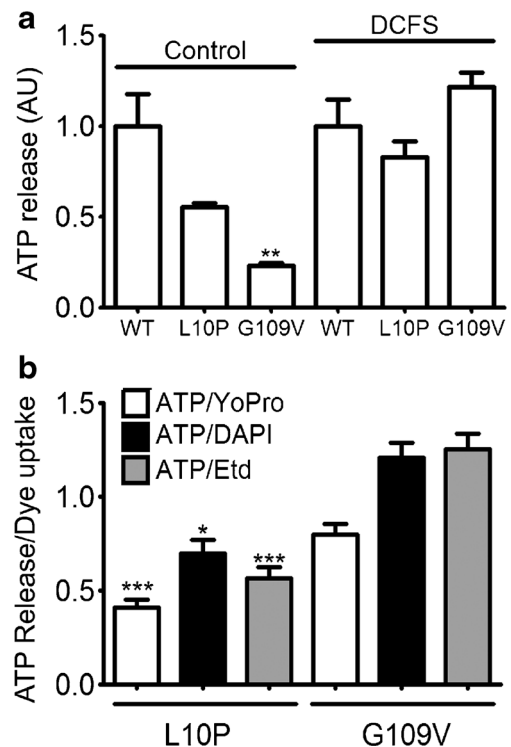

Fig. 4 The effect HC inhibitors on the rate of dye uptake. **a** Cells were exposed to 5 μM DAPI dissolved in DCFS, and the inhibition in response to 1.2 mM Ca^{2+} was determined. **b** Cells were exposed to 5 μM DAPI dissolved in DCFS, and the inhibition in response lowering pH from 7.4 to 6.5 was determined. **c** Cells were exposed to 5 μM DAPI dissolved in DCFS, and the inhibition in response to 200 μM gentamicin was determined. The rate of dye uptake was normalized to the rate in DCFS without inhibitors. Data are means ± SEM of the rate of dye uptake in each cell (four independent experiments for each condition, at least 15 cells analyzed in each experiment). ***$P < 0.001$ compared to the WT Cx26 rate in the same condition
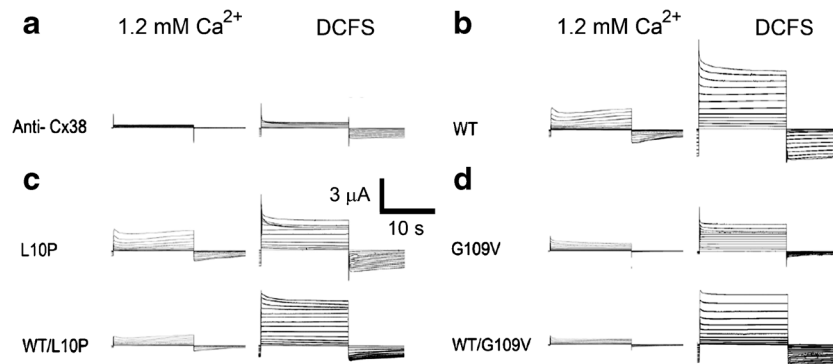
Fig. 6 L10P and G109V form functional voltage-sensitive HCs. **a** Currents recorded in oocytes injected only with anti-Cx38. Data correspond to representative traces obtained in oocytes under the control conditions (ND96 solution containing 1.2 mM Ca^{2+}; 1.2 mM Ca^{2+}) or nominally Ca^{2+}-free ND96 (DCFS). For current measurements, cells were held at −60 mV, and 15-s square pulses were applied (−60 to +60 mV, in 10-mV steps). See Materials and methods for additional details. **b** Currents recorded in oocytes injected with WT Cx26

cRNA plus anti-Cx38 ($n = 15$). See **a** for additional details. **c** Currents recorded in oocytes injected with L10P cRNA plus anti-Cx38 (L10P) ($n = 18$), or co-injected with WT Cx26 and L10P cRNAs (1:1 ratio) plus anti-Cx38 (WT/L10P $n = 15$). See **a** for additional details. **d**. Currents recorded in oocytes injected with G109V cRNA plus anti-Cx38 (G109V) ($n = 9$), or co-injected with WT Cx26 and G109V cRNAs (1:1 ratio) plus anti-Cx38 (WT/G109V; $n = 12$). See **a** for additional details

displayed a more pronounced current inactivation at voltages over +50 mV (Fig. 6b, c, $\tau = 982 \pm 142$ ms), with peak amplitudes not statistically different from those of WT Cx26 (4.92 ± 1.04 μA). When L10P was co-expressed with WT Cx26 (1:1), HC currents were similar to those of WT Cx26 HCs; the only difference was a smaller amplitude in the presence of Ca^{2+} (1.21 ± 0.11 μA, $P < 0.01$ vs. 2.32 ± 0.11 μA for WT Cx26 HCs under the same conditions) (Fig. 6c). G109V HCs were also sensitive to voltage, but both the shape and the amplitude were different from those of WT Cx26 HCs (Fig. 6d). G109V HC currents were smaller under the control conditions (0.83 ± 0.09 μA, $P < 0.005$) and in DCFS (3.03 ± 0.52 μA, $P < 0.05$). Current inactivation at positive voltages was faster than WT Cx26 (Fig. 6d, 450 ± 220 ms). When G109V was co-expressed with WT Cx26 (1:1), the HC current in DCFS (5.08 ± 0.95 μA) was similar to that of WT Cx26 HCs, but the inactivation at positive voltages remained as that of homomeric G109V HCs (Fig. 6d).

The Cx26 L10P mutant forms functional gap-junction channels, but G109V does not

When GJC currents were recorded in *Xenopus* oocytes, there were obvious differences between WT Cx26 and the Cx26 mutants. L10P and WT Cx26/L10P (1:1) formed functional GJCs that displayed currents similar to those of WT Cx26 GJCs (Fig. 7a). However, L10P GJCs showed a different Gj/V relationship (Fig. 7b) and also a more pronounced inactivation at positive voltage, whereas the WT Cx26/L10P inactivation rate was similar to that of WT Cx26 GJCs (Fig. 7a, c). In contrast, expression of G109V and the WT/G109V mix (1:1) did not result in measurable GJC currents (Fig. 7a).
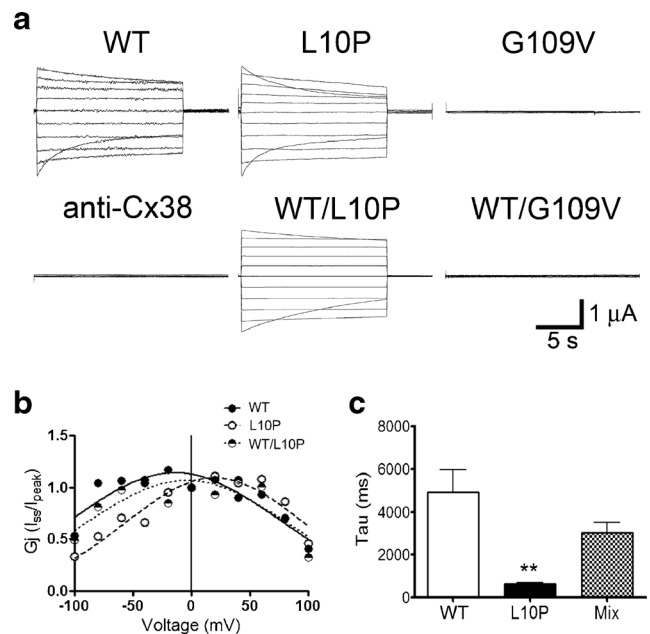

Fig. 7 The G109V mutant does not form functional gap-junctional channels. **a** Typical transjunctional currents (Ij) measured in paired oocytes. Records were obtained in oocytes injected with anti-Cx38 antisense oligonucleotide alone (anti-Cx38) or in combination with cRNA for expression of WT Cx26, L10P, G109V, WT Cx26 plus L10P (Cx26/L10P), or WT Cx26 plus G109V (Cx26/G109V). Paired cells were clamped at −40 mV, and a transjunctional voltage (V$_j$) was generated by stepping the voltage of one cell from −40 mV, while holding constant the voltage of the other cell. The membrane voltage was stepped from −100 to 100 mV, at 20-mV intervals. **b**. Dependence of the average transjunctional conductance (Gj) on transjunctional voltage (Vj). Gj was calculated as the steady-state current (Iss) divided by maximal current ~0.1 s after the onset of the voltage pulse (Ipeak). **c**. Time constants of HC current inactivation (tau) elicited by a −100-mV voltage pulse were calculated from a single-exponential fit to the data and were expressed as means ± SEM ($n = 9$). *Asterisks* denote $P < 0.01$ compared to WT Cx26

Molecular dynamics simulations of WT Cx26 and mutants

All proteins were modeled using the 3.5-Å X-ray structure of Cx26 as template [26]. After 18 ns of simulations, Cx26 HCs displayed an aqueous pore with a narrowest radius of ~10 Å. For the mutants, the narrowest part of the pore was wider, ~12 Å for L10P and ~11 Å for G109V. Based on these results, our models represent a conducting HC state [22]. Figure 8a, b show clear alterations in the mutant HCs' pore structure compared to WT Cx26 HCs. Since L10P and G109V HCs showed altered permeability properties, we analyzed the electrostatic charge of the HC pore surface. Figure 8c shows that WT Cx26 HCs present a relatively neutral/slightly positive area comprised by the extracellular part of the pore and a high density of positive charge inside the pore. In L10P and G109V HCs, both the extracellular region and the pore surface become more positive. These changes in pore structure and electrostatic charges could be involved in the decreased dye uptake and ATP release observed in these two mutants.

Discussion

We have previously identified two novel missense mutations L10P and G109V in the hearing-impaired Argentinean population [11]. The L10P mutation was associated in trans with the V27I variation, a polymorphism [10, 20], whereas G109V was associated in trans with the nonsense mutation E47X. These findings suggest that L10P and G109V are the causes of the deafness in the patients, but functional studies of these mutants were needed to corroborate their potential participation in the phenotype. The present studies support the conclusion that L10P and G109V in Cx26 are the underlying cause of the hearing impairment in those patients, because they show clear effects on GJC and HC activities.

The L10P mutant can form functional GJCs and HCs, albeit with different voltage dependence and solute permeability properties than WT Cx26 HCs. Since L10P forms functional GJCs, it is unlikely that deafness associated with this mutation depends on the lack of electric coupling between cells [19, 33, 44]. This interpretation is consistent with the effect of other Cx26 mutations that display apparently normal electrophysiological properties, but show decrease in permeability to signaling molecules [7]. The absence of currents through G109V or WT Cx26/G109V GJCs clearly point to G109V as a deafness-causing mutant. The absence of transjunctional currents suggests that deafness results from the lack of cell-to-cell communication [19, 30, 40, 44, 47]. The potential mechanism is still unclear. Defective K^+ recycling and cell-to-cell transport of inositol trisphosphate (IP_3) have been proposed as
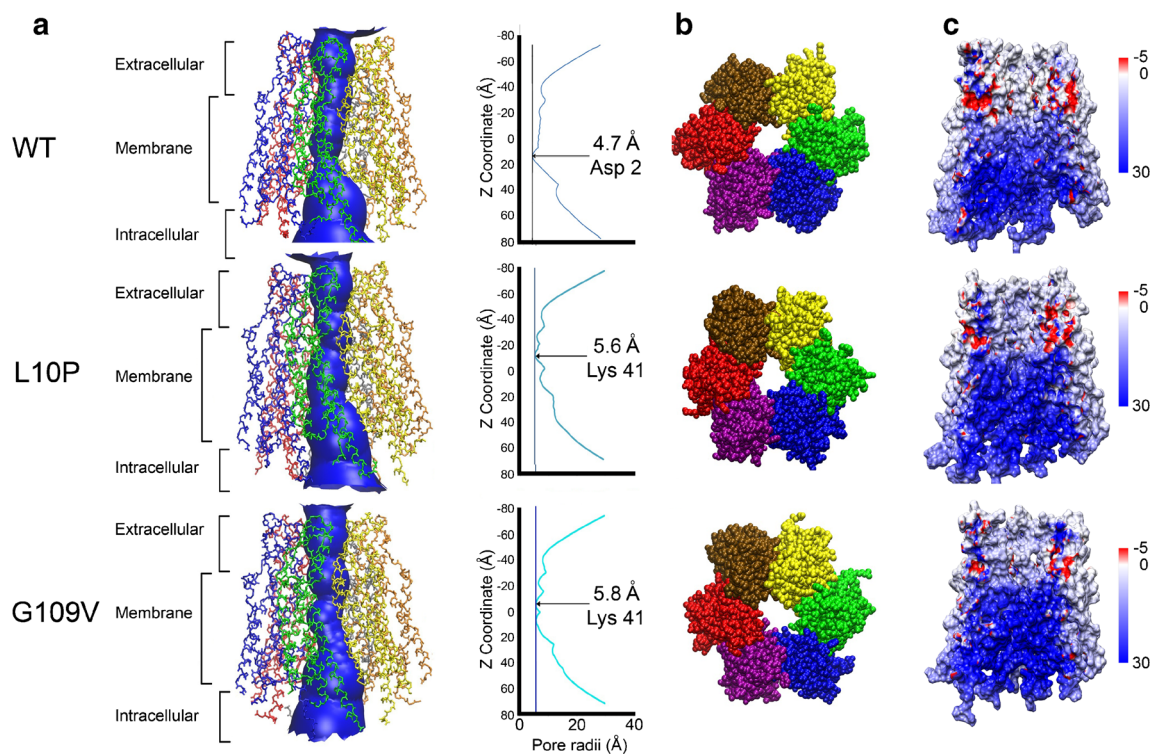

Fig. 8 Cx26 mutations change HC pore shape and charge. a Cartoon representation of the Cx26 HC structure calculated from molecular dynamics modeling using the WT Cx26 crystal structure as template (left). Each connexin subunit was rendered with *different colors*, and the channel pathway is displayed in *blue*. The HC pore radius profile is shown on the right side panels. b HC pore shape viewed from the extracellular side. c Changes of the surface electrostatic potential inside of the channel pore. *Red* indicates negative, *white* neutral, and *blue* positive. In the case of L10P and G109V mutants, the surface of the channel pore becomes more positive, seeing as a *darker blue*

causes of deafness [6, 7, 16, 40, 44]. However, recent studies in Cx26-deficient mouse models showed that K^+-recycling and Ca^{2+}-waves impairment are not responsible for Cx26-induced deafness [45]. In addition, since G109V is expressed at the plasma membrane, but prevents the formation of functional GJCs formed by WT Cx26, we conclude that WT Cx26/G109V is dominant at the GJC level. The ability of G109V to form functional HCs indicates that the absence of functional GJCs does not result from major defects in protein folding or HC assembly. However, subtle alterations in G109V HCs could result in defective docking or formation of impermeable GJCs upon docking (gating defect). The differences in ATP/dye selectivity and voltage dependence point to alterations of G109V HCs compared to WT Cx26 HCs.

According to our MD models, the L10P and G109V mutations result in a small increase in HC pore radius, but induce important changes in the pore structure and surface electrostatic charges. These changes could decrease the permeability of charged molecules through the HC pore. Accordingly, changes in the distribution of charges in the N-terminus change ionic permeability to through Cx32 HCs [31]. The MD simulations support the idea that the L10P and G109V mutations produce distortions in HC structure that can account for the functional effects.

In summary, we described functional effects of two novel deafness-associated Cx26 mutants, L10P and G109V, and showed that L10P is a recessive mutation with subtle effects on GJCs and HCs, whereas G109V prevents formation of functional GJCs in a dominant manner, whereas it still forms functional HCs.

References

1. Anselmi F, Hernandez VH, Crispino G, Seydel A, Ortolano S, Roper SD, Kessaris N, Richardson W, Rickheit G, Filippov MA, Monyer H, Mammano F (2008) ATP release through connexin hemichannels and gap junction transfer of second messengers propagate Ca^{2+} signals across the inner ear. Proc Natl Acad Sci U S A 105:18770–18775

2. Apps SA, Rankin WA, Kurmis AP (2007) Connexin 26 mutations in autosomal recessive deafness disorders: a review. Int J Audiol 46:75–81

3. Baker NA, Sept D, Joseph S, Holst MJ, McCammon JA (2001) Electrostatics of nanosystems: application to microtubules and the ribosome. Proc Natl Acad Sci U S A 98:10037–10041

4. Bao X, Altenberg GA, Reuss L (2004) Mechanism of regulation of the gap junction protein connexin 43 by protein kinase C-mediated phosphorylation. Am J Physiol Cell Physiol 286:C647–C654

5. Bargiello TA, Tang Q, Oh S, Kwon T (2012) Voltage-dependent conformational changes in connexin channels. Biochim Biophys Acta 1818:1807–1822

6. Beltramello M, Piazza V, Bukauskas FF, Pozzan T, Mammano F (2005) Impaired permeability to Ins(1,4,5)P3 in a mutant connexin underlies recessive hereditary deafness. Nat Cell Biol 7:63–69

7. Bruzzone R, Veronesi V, Gomes D, Bicego M, Duval N, Marlin S, Petit C, D'Andrea P, White TW (2003) Loss-of-function and residual channel activity of connexin26 mutations associated with non-syndromic deafness. FEBS Lett 533:79–88

8. Chen J, Chen J, Zhu Y, Liang C, Zhao HB (2014) Deafness induced by connexin 26 (GJB2) deficiency is not determined by endocochlear potential (EP) reduction but is associated with cochlear developmental disorders. Biochem Biophys Res Commun 448: 28–32

9. Chen Y, Deng Y, Bao X, Reuss L, Altenberg GA (2005) Mechanism of the defect in gap-junctional communication by expression of a connexin 26 mutant associated with dominant deafness. FASEB J 19:1516–1518

10. Choi SY, Lee KY, Kim HJ, Kim HK, Chang Q, Park HJ, Jeon CJ, Lin X, Bok J, Kim UK (2011) Functional evaluation of GJB2 variants in nonsyndromic hearing loss. Mol Med 17:550–556

11. Dalamón V, Lotersztein V, Béhèran A, Lipovsek M, Diamante F, Pallares N, Francipane L, Frechtel G, Paoli B, Mansilla E, Diamante V, Elgoyhen AB (2010) GJB2 and GJB6 genes: molecular study and identification of novel GJB2 mutations in the hearing-impaired Argentinean population. Audiol Neuro Otol 15:194–202

12. Figueroa VA, Retamal MA, Cea LA, Salas JD, Vargas AA, Verdugo CA, Jara O, Martínez AD, Sáez JC (2014) Extracellular gentamicin reduces the activity of connexin hemichannels and interferes with purinergic Ca(2+) signaling in HeLa cells. Front Cell Neurosci 8: 265

13. Fiori MC, Figueroa V, Zoghbi ME, Saéz JC, Reuss L, Altenberg GA (2012) Permeation of calcium through purified connexin 26 hemichannels. J Biol Chem 287:40826–40834

14. Gerido DA, DeRosa AM, Richard G, White TW (2007) Aberrant hemichannel properties of Cx26 mutations causing skin disease and deafness. Am J Physiol Cell Physiol 293:C337–C345

15. Gómez-Hernández JM, de Miguel M, Larrosa B, González D, Barrio LC (2003) Molecular basis of calcium regulation in connexin-32 hemichannels. Proc Natl Acad Sci U S A 100: 16030–16035

16. Gossman DG, Zhao HB (2008) Hemichannel-mediated inositol 1, 4,5-trisphosphate (IP3) release in the cochlea: a novel mechanism of IP3 intercellular signaling. Cell Commun Adhes 15:305–315

17. Harris AL, Locke D (2009) Permeability of connexin channels. In: Harris AL, Locke D (eds) Connexins: a guide. Humana Press, New York, pp 165–206, **Chapter 7**

18. Humphrey W, Dalke A, Schulten K (1996) VMD: visual molecular dynamics. J Mol Graph 14:33–38

19. Johnstone BM, Patuzzi R, Syka J, Sykova E (1989) Stimulus-related potassium changes in the organ of Corti of guinea-pig. J Physiol 408:77–92

20. Kelley PM, Harris DJ, Comer BC, Askew JW, Fowler T, Smith SD, Kimberling WJ (1998) Novel mutations in the connexin 26 gene (GJB2) that cause autosomal recessive (DFNB1) hearing loss. Am J Hum Genet 62:792–799

21. Kudo T, Kure S, Ikeda K, Xia AP, Katori Y, Suzuki M, Kojima K, Ichinohe A, Suzuki Y, Aoki Y, Kobayashi T, Matsubara Y (2003) Transgenic expression of a dominant-negative connexin26 causes degeneration of the organ of Corti and non-syndromic deafness. Hum Mol Genet 12:995–1004

22. Kwon T, Harris AL, Rossi A, Bargiello TA (2011) Molecular dynamics simulations of the Cx26 hemichannel: evaluation of structural models with Brownian dynamics. J Gen Physiol 138:475–493

23. Lee JR, Derosa AM, White TW (2009) Connexin mutations causing skin disease and deafness increase hemichannel activity and cell death when expressed in Xenopus oocytes. J Invest Dermatol 129:870–878

24. Liang C, Zhu Y, Zong L, Lu GJ, Zhao HB (2012) Cell degeneration is not a primary cause for connexin26 (GJB2) deficiency associated hearing loss. Neurosci Lett 528:36–41

25. Liu W, Boström M, Kinnefors A, Rask-Andersen H (2009) Unique expression of connexins in the human cochlea. Hear Res 250:55–62

26. Maeda S, Nakagawa S, Suga M, Yamashita E, Oshima A, Fujiyoshi Y, Tsukihara T (2009) Structure of the connexin 26 gap junction channel at 3.5 A resolution. Nature 458:597–602

27. Majumder P, Crispino G, Rodriguez L, Ciubotaru CD, Anselmi F, Piazza V, Bortolozzi M, Mammano F (2010) ATP-mediated cell-cell signaling in the organ of Corti: the role of connexin channels. Purinergic Signal 6:167–187

28. Martínez AD, Acuña R, Figueroa V, Maripillan J, Nicholson B (2009) Gap-junction channels dysfunction in deafness and hearing loss. Antioxid Redox Signal 11:309–322

29. Meşe G, Richard G, White TW (2007) Gap junctions: basic structure and function. J Invest Dermatol 127:2516–2524

30. Nickel R, Forge A, Jagger D (2009) Connexins in the inner ear. In: Harris AL, Locke D (eds) Connexins: a guide. Humana Press, New York, pp 419–434, **Chapter 20**

31. Oh S, Verselis VK, Bargiello TA (2008) Charges dispersed over the permeation pathway determine the charge selectivity and conductance of a Cx32 chimeric hemichannel. J Physiol 586:2445–2461

32. Philips JC, Braun R, Wang W, Gumbart J, Tajkhorshid E, Villa E et al (2005) Scalable molecular dynamics with NAMD. J Comput Chem 26:1781–1802

33. Rabionet R, Zelante L, López-Bigas N, D'Agruma L, Melchionda S, Restagno G, Arbonés ML, Gasparini P, Estivill X (2000) Molecular basis of childhood deafness resulting from mutations in the GJB2 (connexin 26) gene. Hum Genet 106:40–44

34. Retamal MA, Evangelista-Martínez F, León-Paravic CG, Altenberg GA, Reuss L (2011) Biphasic effect of linoleic acid on connexin 46 hemichannels. Pflugers Arch 461:635–643

35. Retamal MA, Reyes EP, García IE, Pinto B, Martínez AD, González C (2015) Diseases associated with leaky hemichannels. Front Cell Neurosci 9:267

36. Retamal MA, Schalper KA, Shoji KF, Bennett MV, Sáez JC (2007) Opening of connexin 43 hemichannels is increased by lowering intracellular redox potential. Proc Natl Acad Sci U S A 104:8322–8327

37. Sáez JC, Schalper KA, Retamal MA, Orellana JA, Shoji KF, Bennett MV (2010) Cell membrane permeabilization via connexin hemichannels in living and dying cells. Exp Cell Res 316:2377–2389

38. Sanchez HA, Bienkowski R, Slavi N, Srinivas M, Verselis VK (2014) Altered inhibition of Cx26 hemichannels by pH and Zn^{2+} in the A40V mutation associated with keratitis-ichthyosis-deafness syndrome. J Biol Chem 289:21519–21532

39. Sanchez HA, Villone K, Srinivas M, Verselis VK (2013) The D50N mutation and syndromic deafness: altered Cx26 hemichannel properties caused by effects on the pore and intersubunit interactions. J Gen Physiol 142:3–22

40. Steel KP (1999) Perspectives: biomedicine. The benefits of recycling. Science 285:1363–1364

41. Stong BC, Chang Q, Ahmad S, Lin X (2006) A novel mechanism for connexin 26 mutation linked deafness: cell death caused by leaky gap junction hemichannels. Laryngoscope 116:2205–2210

42. Terrinoni A, Codispoti A, Serra V, Didona B, Bruno E, Nisticò R, Giustizieri M, Alessandrini M, Campione E, Melino G (2010) Connexin 26 (GJB2) mutations, causing KID Syndrome, are associated with cell death due to calcium gating deregulation. Biochem Biophys Res Commun 394:909–914

43. Verselis VK, Srinivas M (2008) Divalent cations regulate connexin hemichannels by modulating intrinsic voltage-dependent gating. J Gen Physiol 132:315–327

44. Wangemann P (2006) Supporting sensory transduction: cochlear fluid homeostasis and the endocochlear potential. J Physiol 576:11–21

45. Wingard JC, Zhao HB (2015) Cellular and deafness mechanisms underlying connexin mutation-induced hearing loss—a common hereditary deafness. Front Cell Neurosci 9:202

46. Zelante L, Gasparini P, Estivill X, Melchionda S, D'Agruma L, Govea N et al (1997) Connexin26 mutations associated with the most common form of non-syndromic neurosensory autosomal recessive deafness (DFNB1) in Mediterraneans. Hum Mol Genet 6:1605–1609

47. Zhao HB, Kikuchi T, Ngezahayo A, White TW (2006) Gap junctions and cochlear homeostasis. J Membr Biol 209:177–186

48. Zhu Y, Chen J, Liang C, Zong L, Chen J, Jones RO, Zhao HB (2015) Connexin26 (GJB2) deficiency reduces active cochlear amplification leading to late-onset hearing loss. Neuroscience 284:719–729

49. Zhu Y, Liang C, Chen J, Zong L, Chen GD, Zhao HB (2013) Active cochlear amplification is dependent on supporting cell gap junctions. Nat Commun 4:1786

50. Zoidl G, Dermietzel R (2010) Gap junctions in inherited human disease. Pflugers Arch 460:451–466